Highlights

- The use of a pressure mapping system for capturing wave impact induced pressures on a vertical structure is validated against pressure transducer and load cell measurements.
- An encouraging agreement is reported for the spatial distribution and the magnitudes of the pressure peaks captured by the system and pressure transducer arrays.
- The integral of the pressures recorded by the system is compared with simultaneous load cell measurements and errors smaller than ±20% are reported for the majority of the tests.
- Overall, the results presented encourage the use of the system for acquiring insights on the spatial structure of wave impact induced pressures.

.

Measuring wave impact induced pressures with a pressure mapping system

DIMITRIS STAGONAS [(1)], ANDREA MARZEDDU [(2)], FRANCESC XAVIER GIRONELLA I COBOS [(2)], AGUSTIN SÁNCHEZ-ARCILLA CONEJO [(2)], GERALD MULLER[(3)]

(1) University College of London, Department of Civil, Enviromental and Geomatic engineering Gower St, London WC1E 6BT, United Kingdom. d.stagonas@ucl.ac.uk

(2) Laboratorio de Ingeniería Marítima (LIM), Universitat Politecnica de Catalunya, Barcelona 08034, Spain, andrea.marzeddu@upc.edu

(3) University of Southampton, Faculty of Engineering and the Environment Gower St, London WC1E 6BT, United Kingdom. d.stagonas@ucl.ac.uk

Abstract

The use of a pressure mapping system for measuring wave impact induced pressures is evaluated in this paper. A set-up and a calibration methodology are suggested and employed for this work . The system is validated against pressure transducer and load cell measurements and for a range of waves breaking on a vertical seawall. For a large number (120 measurements for each case considered) of breaking and broken waves interacting with the wall, the peak pressure (P_{peak}) profiles and the pressure distribution maps reported by the system agree well with results acquired using pressure transducers. Although the pressure mapping system tends to underestimate P_{peak}, differences on the mean of the 3, 5 and 10 highest P_{peak} range within ±10%, while for the majority of the measurements the error on the integral of the acting pressures (the acting force compared with the force measured by the load cell) ranges within ±20%. It is concluded, that through careful calibration and set-up the pressure mapping system has the capacity to provide pressure distribution maps with a good accuracy. It is not, however, consider to constitute the absolute alternative to pressure transducers and thus a combined use is suggested for applications where a very high level of accuracy is required.

Keywords: Pressure Mapping System; Wave Impacts; Pressure distribution; Pressure/Force measurements;

1 Introduction

As knowledge on the mechanics involved in the breaking wave-structure interaction is limited impact induced pressure measurements are one of the most important outcomes expected from hydraulic model tests. Pressure measurements are usually preferred over load measurements as they allow for the detection of vulnerable areas on the structure, while the acquisition of global loads requires at times complicated and expensive experimental layouts, especially in large scale facilities. For most physical model tests involving, e.g., coastal structures an array of pressure transducers is placed vertically at the seaward face of the structure and the data collected are used for the construction of pressure profiles and the calculation wave induced loads and moments, Cuomo et al. (2010).

Nonetheless, pressure transducers provide single point measurements and in most cases a relatively small number of transducers is used. In the same time, the high spatial and temporal variability of wave impact induced pressures, Hattori (1994), Peregrine (2003), Saruwatari et al. (2009), the limited information available even on the coherence pressure profiles, Hull and Möller (2002), and the increased complexity on the geometry of the structures (for example, wave re-curves, wave energy

converters and ships) tested, drive the need for experimental measurements with a high spatial resolution.

Additional challenges emerge when cylinders and structures with more complex geometrical shapes are considered. For example, investigating the survivability of wave energy converters, offshore oil platforms or wave recurves requires detailed knowledge of the impact induced pressure distribution. However, due to technical and financial restrictions high resolution pressure maps cannot be produced using pressure transducers.

A pressure mapping system with the potential to provide pressure measurements with a high spatial resolution is described in section 2. The system has been used in and validated for, e.g., biomedical and geotechnical applications but never before for measuring wave induced impact pressures. Nevertheless, the existing literature suggests that the accuracy of the system depends strongly on the experimental set-up and the calibration methodology employed, Baer et al. (2004) and Brimacombe et al. (2009). Therefore a calibration set-up and methodology designed for application in hydraulic model tests with waves breaking on a rigid structure are proposed. The performance of the system is evaluated against pressure transducer and load cell measurements for a wide range of breaking conditions on a vertical seawall model in section 3 and the work is concluded in section 4.

2 Methodology

2.1 Experimental equipment

2.1.1 Pressure mapping system

The high speed Tekscan Pressure Mapping System (PMS) is used here. The system consists of a tactile pressure sensor (sometime referred to as pressure pad or simply pad), a connection handle and a hub allowing the simultaneous use of more than one handles and triggering from an external signal. The hub is connected to the USB port of any PC equipped with I-Scan software provided by the manufacturer along with the PMS.

A variety of tactile pressure sensors is available with their characteristics ranging in terms of number of measuring points (most commonly referred to as sensels), physical size and maximum sampling frequency. For all tests presented here the tactile sensor with model number 9500 was used. The sensor has 196 sensels spread at equal distances over a square area of 7.1x7.1cm and it allows for a maximum sampling frequency of 4 kHz with and 8bit resolution. At this point it should be highlighted that each sensel consists of an active and a ‘dead’ area with the latter surrounding the former. An intrinsic disadvantage is thus entailed, since the pressure is calculated as force over the full (active and ‘dead’) area of each sense. The pressure mapping system is not provided already calibrated by the manufacturer and its calibration prior to any test is recommended.

The calibration rig developed specifically for this work is presented in **Figure 1**. The Tekscan sensor is firmly fixed below a tube (not shown in **Figure 1**), on a 3mm thick aluminum plate. As the sensor is not water-proof adequate protection from water is provided by placing the sensor in a vacuum bag (Minimatic bag 0.05 mm) and a secondary protection layer is created using a transparent, deformable/compliant foil (vacuum film NBF-740-LFT 0.05 mm). A vacuum pump is used to reassure that air is not trapped in the tactile sensor and between the sensor and the protection layers, and the vacuum pressure acting on the sensor is removed from the measurements during the post-processing. If not properly removed, entrapped air can significantly deteriorate the accuracy of system, see Tekscan (2008) and **Ramachandran et al. (2013)**. Nevertheless, **Ramachandran et al. (2013)** has shown that once the formation of unwanted air pockets is prevented the response of the sensor remains the same for different vacuum levels but for all measurements presented here a constant vacuum of 40kPa was maintained. This was indicated in preliminary tests to be the minimum

vacuum required to remove all air and generate a homogenous pressure field on the sensor. It is noteworthy, that the vacuum pump was found to introduce a high frequency (25Hz) noise to the signal but a low pass filter was also found to be very effective on removing it.

Impinging water-jets are used to induce dynamic pressures on the sensels of the tactile pressure sensor. The pressure pulses generated by impinging water jets resemble very closely those expected in experiments with waves breaking on rigid structures, see for example **Figure 9** and **Figure 10**. During the first moments of the impact a sharp increase from 0 to peak pressure occurs and subsequently the pressure decreases as the phenomenon transcends from a dynamic to a quasi-static phase.

The impact induced load is measured using a pair of HBM Z6FC3 bending beam load cells arranged in series, **Figure 1** but for each impact the area (*A*) is simultaneously measured by the Teskan sensor, **Figure 2** (on the left). Accordingly, the mean pressure (P_{LC}) acting on the sensor is calculated as the ratio of the force recorded by the load cells over the area measured by the tactile pressure sensor, eq. 1 & 2.

$$A = N * A_{sensel} \quad \textbf{Eq. 1}$$

where,

- N: is the number of active sensels
- A_{sensel}: is the sensel area, equal to 26 mm2

and is used to calculate the mean pressure from the load cell measurement, as:

$$P_{LC} = \frac{F_{PLC}}{A} \quad \textbf{Eq. 2}$$

where,

- F_{PLC}: is the peak force measured by the load cell
- P_{LC}: is the mean pressure acting on the tactile sensor at the time F_{PLC} occurs

The digital output of a sensel is the considered equal to the calculated pressure multiplied by a weighting factor, eq. 3 & 4.

$$C_{i,j} = 1 - \frac{\overline{DO} - DO_{i,j}}{\overline{DO}} \quad \textbf{Eq. 3}$$

where,

- $C_{i,j}$: is the contribution factor for a sensel with horizontal (x) and vertical (y) coordinates i, j, respectively. With i = 1…14 and j = 1…14.
- $DO_{i,j}$: is the digital output of a sensel with horizontal (x) and vertical (y) coordinates i, j.
- $\overline{DO}$: is the mean of the digital output of all sensels active at the time instant the peak force was recorded by the load cells.

The combination of Eq. 1 to 3 gives the weighted pressure, $P_{i,j}$, acting on the (i,j) sensel:

$$P_{i,j} = C_{i,j} * P_{LC} \quad \textbf{Eq. 4}$$

For this work, the sensor was calibrated using 300 water jet impacts and the digital output of a sensel is plotted as a function of $P_{i,j}$, **Figure 2** (on the right). The lines plotted correspond to a linear (dashed),

a power law (solid) and a 2nd order polynomial fit (dotted), and represent three different calibration algorithms. When the integral of the pressures acting on each sensel was compared with the load cell measurements statistically indistinguishable results were found for all algorithms, **Table 1**

	RMSE [N]		
	min	**mean±std**	**max**
Linear	0.0012	1.47±1.23	6.7
2nd order	0.0021	1.49±1.23	6.72
Power law	0.0053	1.49±1.23	6.7

Table 1: RMSE of the integral of the pressure acting on each sensel for the three calibration methods

Nevertheless, the manufacturer recommends the use of a non-linear power law algorithm which was also preferred for this work, Tekscan (2008).

Overall, the calibration rig of Figure 1 was designed to generate conditions similar to those anticipated in the experiments. The proposed arrangement ensures the protection of the sensor from direct contact with water and prevents unwanted entrapped air effects. Finally, consistency between the calibration and experiments is maintained by applying the same set-up for the tactile pressure sensor.

2.1.2 Pressure transducers and load cells

In total, 8 P8AP pressure transducers were available. The P8AP is an absolute pressure transducer suitable for measuring static and dynamic, gas or liquid induced pressures and can be safely immersed to depths down to 1m. Each transducer is composed of a strain-gauge sensor and is provided already calibrated by the manufacturer (HBM); accompanied with a CE declaration of conformity and a test certificate. The P8AP sensors used here have a maximum measuring range of 103kN/m^{2}with a reported accuracy of 0.3% of the maximum load, a 24bit resolution and a natural frequency of the diaphragm of 12 KHz.

Force measurements were conducted using two Z6FC3 bending beam load cells with a nominal load of 50Kg, an accuracy of 0.009% of the maximum load and a resolution of 24bit. As for the pressure transducers the load cells are provided calibrated and they can be immersed to a maximum depth of 1m. An HBM QuantumX data acquisition system is used to simultaneously sample each load cell and pressure transducer with a sampling frequency of 4.8 kHz. Although the system has the capacity to amplify and sample up to 16 channels with a maximum sampling rate of 19.2 kHz, 4.8 kHz were selected as the rate closest to that of the pressure mapping system (4 kHz per sensel). For experiments with pressure transducers Marzeddu et al. (2013, 2014) recorded the highest impact pressure with a sampling frequency of 19.2 kHz but they concluded that a satisfactory description of the pressure pulse can be acquired with a minimum of 2.4 kHZ.

2.1.3 Experimental setup

All experiments were carried out in the CIEMito wave flume of the Laboratori d'Enginyeria Maritima (LIM) of the Universitat Politecnica de Catalunya BarcelonaTech (UPC). The flume is 18m long, 0.38m wide and 0.56m deep and a vertical seawall model is placed at the end of a 1:15 smooth slope, Figure 3.

Groups of regular waves are generated by a computer driven piston type wave maker. For each group the first (ramp-up) wave is always smaller than the target wave height and it is fully reflected at the structure, while the second wave has the height reported in Table 2 and results in an impact at the wall. Through small variations of the water depth (d), the wave height (H) and period (T) different breaking conditions are induced on the wall, see Table 2. Broken waves were generated by introducing a 0.2×0.35×0.05m (length×width×depth) block 0.5m from the structure.

H [m]	T [s]	d [m]	N. Repetitions	Breaker type	RMSE [m]	Error [%]
0.16	2.4	0.285	120	Nearly breaking (NB)	0.003	2

0.16	2.3	0.285	120	Large air pocket (LP)	0.004	2.5
0.16	2.3	0.29	120	Small air pocket (SP)	0.003	1.8
0.16	2.3	0.285	120	Broken wave (BW)	0.004	2.5

Table 2: Incoming wave parameters and RMSE and percentage of error on surface elevation measurements for 120 waves of each category. The wave height error calculation were computed from wave probe number 1 at 3 m from the wavemaker.

Each breaker type is repeated 120 times. As the 1st wave of the group is always reflected at the structure the impact of the 2nd wave was considered to be the cleanest and most repeatable. For this reason, only the pressures induced by the impact of this wave on the seawall are considered. The repeatability on the generation of the wave groups was also tested and the RMSE (computed on wave height) and percentage of error values are also shown in Table 2.

In total, 4 experimental arrangements EA1 to EA4 are employed for this work and the Tekscan I-ScanTM pressure mapping system is validated through the cross-comparison of the different data sets produced. For EA1 the tactile sensor is placed on top of segment of the vertical wall mounted on a load cell, Figure 4. The load cell has a high stiffness and it is in turn mounted on a stiff metallic structure. The segment of the wall is of the same size (7.1 x 7.1 cm) as the tactile sensor and the water-proofing arrangement used for calibration is utilised, Figure 1.

For EA2, and array of 7 pressure transducers is placed in the middle of the vertical wall. The vertical intervals between the transducers (PT1 to PT3 and PT5 to PT8 near the top of the wall) are shown in Figure 4, while an additional transducer (PT4 in Figure 4) is placed near SWL and at a distance of 2.5 cm to the left of the array. As for *EA1*, the array is mounted on a segment of the wall (35 x 10 cm) supported this time on two load cells, see Figure 4.

In contradiction to *EA1* and *EA2* a not-segmented seawall model is used for *EA3* and matrix of 13 measuring locations is created at the same location as the tactile sensor for *EA1*, Figure 4. Restrictions due to the physical dimensions of the transducers make the simultaneous use of load cells impossible. In addition, and since no more than 7 transducers can be fit on the area of interest 120 impacts of each breaker type are recorded and the tests are repeated with 6 transducers re-located on the remaining 6 positions. This way, a matrix of 13×120 measurements is generated.

Given the aims of this paper, *EA1* allows for the comparison of force measurements acquired by the tactile sensor with simultaneous load cell measurements, while the vertical distribution of the peak pressures (P_{peak}) recorded by the pressure mapping system for *EA1* is evaluated against the transducer measurements for *EA2*. For *EA1* and *EA2* the same incoming wave conditions are used and pressure records are acquired for segments of the wall mounted on load cells.

Nevertheless, impact induced pressures for *EA3* are measured on a non-segmented wall and therefore *EA4* is utilised to evaluate potential effects of the latter difference. For *EA4*, a segment of the seawall model equal in size to that for *EA1* is mounted on the load cell and 4 pressure transducers are fixed near the 4 corners of the plate as shown in Figure 4; pressure transducer positions for *EA2* (small circles), *EA3* (small circles) and *EA4* (small circles) are also shown in Figure 4.

Indicative results for the comparison between *EA3* and *EA4* for breaking waves with large air pocket(LP) and broken waves (BW) are presented in Figure 5, where the P_{peak} probability of non-exceedance is plotted for *EA3* (circles) and *EA4* (triangles). For breaking waves, the peaks of the pressures recorded for *EA3* are up to 3.5 times higher than those for *EA4* but they are reported to range within the same order of magnitude for broken waves; similar trends were seen when *EA3* was compared with *EA2* and *EA1* (comparison not presented here). The results of Figure 5 are not investigated further within this work but they are used in support of those (results) presented in section 3.1.2.

3 Results and discussion

3.1.1 Vertical distribution and pressure rise time

Hull and Muller (2002), have shown that for waves shoaling over a slope and breaking on a vertical wall maximum impact pressures are located at and near Still Water Level (SWL). This was later on confirmed by several researchers conducting tests in similar or larger scales, see for example Kisacik et al. (2012), Bullock et al. (2007) and Cuomo et al. (2010).

The vertical distribution of the highest peak pressures (P_{peak}) measured by 14 vertical arrays of 14 sensels (dashed grey to black lines) is compared with those reported by the array of 7 pressure transducers (solid black line)in Figure 6.

A reasonable agreement is observed between the pressure profiles induced by breaking waves forming a large air pocket (left subplot) and broken waves (right subplot). For both instruments, and in line with previous works, the highest pressures are located at and slightly above SWL. Sensels positioned at locations similar (dashed black line with P_{peak} = 82kPa on the left hand side of Figure 6) to those of the pressure transducers report the highest P_{peak} for (z-d)/H = 0.18, which is increased by 14% compared to the P_{peak} for the transducer array. In principle, profiles with increased P_{peak} (grey and light grey lines) are reported for sensel arrays the coordinates of which do not overlap with those of the pressure transducer array. It is however noteworthy that all profiles maintain a coherent shape as P_{peak} values on each side of the maximum P_{peak} decrease gradually. Broken wave impacts result in more irregular pressure profiles with reduced coherence but a reasonably good overall agreement between the pressure profiles is still observed.

Pressure transducers PT3, PT4, PT5 and PT6 are located inside the impact zone for breaking and broken waves and the P_{peaks} recorded for 120 impacts are compared with measurements from sensels at similar locations in Figure 7 and Figure 8.

The quantiles calculated for each data set are shown in the Quantile-Quantile plots (QQplot) of Figure 7 and Figure 8 along with a reference (dashed) line joining the 1st and 3rd quartile of each distribution. Since the majority of the plotted quantiles form the line it can be said that the data recorded by the sensels and those recorded by the pressure transducers come from the same distribution family and they have similar mean and standard deviation (STD).

Indeed, and for example, the mean and STD for PT4 and PT5 and the corresponding sensels is 28.43kPa and 10.88, 39.3kPa and 11.05, and 23.58kPa and 13.98, 33.04kPa and 12.4, respectively. Similar results are found for PT3 and PT6, while for broken waves the mean and STD are 5.62kPa and 1.9, 4.9kPa and 1.53, and 5.89kPa and 2.07, 4.88kPa and 2.02. Nonetheless, the mean of the recorded P_{peak} is of little value from a design point of view, for which the highest values of P_{peak} are more useful. The average of the 3, 5 and 10 highest P_{peak} for PT4 and PT5 and breaking waves is 63.2kPa, 60.02kPa and 54.54kPa, and 68.27kPa, 64.6kPa and 61.1kPa, while for the sensels of the tactile sensor is 65.7kPa, 61.8kPa and 56.8kPa, and 74.4kPa, 71.2kPa, and 65.13kPa, respectively.

The $y=ax$ (black solid) line is also plotted in Figure 7 and Figure 8. Although a reasonable agreement between sensels and pressure transducers is seen for the aforementioned mean and highest P_{peak} the vast majority of quantiles fall above the $y=ax$ line. Thus a tendency of the pressure mapping system to underestimate pressures is clearly indicated. Given the similar sampling rates (4kHz for the tactile sensor and 4.8kHz for the pressure transducers) and the large number of impacts considered this tendency can be attributed to the low digital resolution of the tactile sensor and to calibration inaccuracies. In addition the largest discrepancies refer to the smaller P_{peak} measured. This is in-line to results presented in the literature for a variety of different applications showing that the accuracy of the Tekscan tactile sensors reduces for pressures closer the lower end of the their nominal range.

On the other hand, Kim et al. (2015) compared the performance of pressure sensors for sloshing induced impact pressures. Interestingly enough, the authors presented measurements showing that two ICP (Integrated Circuit Piezoelectric) sensors of the same type, the sensing diameter and linearity return different results on peak pressure measurements; the characteristics of both ICP sensors are similar to those of the pressure transducers used here. Kim et al. (2015) presented also pressure pulse time histories for both ICP sensors and highlighted differences on the sharpness/spikiness of the pressure signal, pressure drops and significant differences on rise time measurements.

Pressure time history examples for pressure transducers and sensels located above and below SWL are illustrated in Figure 9. It is noteworthy that a signal drift is not observed for the tactile sensor time histories shown on the lefts hand side of Figure 9. When focusing in the details of a single impact, Figure 10, it becomes apparent that high frequency oscillations are not reported by the sensels of the pressure mapping system. Such high frequency oscillations have been associated with the presence of air bubbles entrained in the fluid during the impact, and can be clearly observed in the pressure transducer time histories.

In the same time histories, the rise time (t_r) is defined as the time required for the pressure to increase from 0 to its peak value. The rise time is linked to the response for the structure and its importance in the design process of, e.g., coastal structures is emphasised in contemporary design guidelines, Oumeraci et al. (2001). All t_r measurements for pressure transducers (crosses) and sensels (circles) are presented in Figure 11 as a function of P_{peak}.

Overall, the exponential relation (the rise time increases as the pressure reduces) between P_{peak} and t_r observed for the pressure mapping system is in good qualitative agreement with that reported for the pressure transducer measurements but also with that presented elsewhere for similar experiments, see for example Kisacik et al. (2012). In principle, however, shorter rise times are seen for the tactile sensor and the average of t_r for the 3, 5 and 10 highest P_{peak} recorded for LP (breaking wave forming a large air pocket with the wall) range between 1.8ms and 2ms, and 1.3ms and 1.4ms for PT4 and PT5, and 0.6-1.2ms for the corresponding sensels.

The differences in t_r can be attributed to disadvantages explicit to the *Tekscan I-Scan*^{TM} pressure mapping system, like the low digital resolution (8bit). The latter entails that a smaller number of measurements is available to capture the (rapidly increasing) rising part of the pressure pulse resulting in a sharper and overall poorer description. The effect of the sampling frequency on the comparison between the two instruments is considered to be negligible as a similar rate is used; 4kHz (the maximum available rate the model 9500 tactile sensor) for the pressure mapping system and 4.8kHz for the pressure transducers.

On the other hand, the definition of the rise time used here in combination with the shape of the pressure time history records can also introduce errors. Very recently Kim et al. (2015) reported differences (up to 100%) on t_r measurements conducted by two pressure transducers with similar technical specifications but natural frequencies of 250kHz and 300kHz, respectively. These were attributed to alterations on the shape of the time history prior to P_{peak}, e.g. negative signal drops, due to thermal shocks and/or sudden medium changes (air to water).

In summary, the discrepancies on tr measurements presented (Figure 11) and discussed are not considered significant enough in order to disregard the use of the *Tekscan I-Scan*^{TM} pressure mapping system.

3.1.2 Pressure distribution map

The high spatial variability of impact induced pressures is by now well recognised, see for example Hofland et al. (2010) and Stansberg et al. (2012), but the mechanisms of the wave impact on a structure remain largely unknown and thus the distribution of impact pressures unpredictable. Accordingly the capability of the pressure mapping system to provide high resolution maps of the

impact induced pressure distribution becomes appealing. In this section, the distribution map of the maximum P_{peak} recorded by the pressure mapping system is compared with measurements by 3 vertical arrays of pressure transducers and a first evaluation step is made.

An example of the pressure map time history for a breaking wave is given in Figure 12, where the instantaneous pressure measurements for all sensels are illustrated as contour plots.

In agreement with previous works, the highest pressures are seen to occur near SWL but their spatial distribution is seen to vary with time. This spatial and temporal variability of impact induced pressures is potentially associated to the shape of the wave crest during breaking, see for example Peregrine (2003) and Saruwatari et al. (2009).

The map of the highest pressures recorded by all sensels (*EA1*) for 120 impacts is compared with pressure transducer measurements (*EA3*) in Figure 13. Two different arrangements (7 and 6 transducers respectively) and 2×120 wave impacts were used to construct the matrix on the right hand side of Figure 13. For EA3 pressures were measured on a solid wall while for every other arrangement impact pressures were measured on a segment of the wall mounted on load cells. The comparison between EA1, EA2 and EA4 (see section 2) clearly shows that for the tests with a solid wall the magnitudes of the impact pressures induced for the same incoming wave conditions are consistently higher; P_{peak} within the impact zone for EA3 are up to 3.5 times higher than those for EA2 and EA4.

With that in mind, a reasonable qualitative agreement can be observed for the results presented in Figure 13. The maximum P_{peak} recorded by each sensel (image on the left) and pressure transducer (image on the right) for 120 and 2×120 impacts of a breaking wave is plotted in Figure 13 as a function of each instruments location. The distance from the side wall is used for x (horizontal), y coordinates (vertical) are presented in relevance to the water depth, and the color scale (white to black) corresponds to increasing values of P_{peak}. For both sensors the impact zone is located above SWL although for the pressure transducers it appears to extend up to about z/d=1.35 instead of z/d=1.3 for the PMS. However, this small discrepancy is justifiable by the differences on the positioning, size and shape of the measuring area of sensels and transducers.

The impact zone is very clearly depicted by the tactile sensor and maximum peak pressures (dark grey to black) occur for $0.14 \leq x \leq 0.15$, $0.17 \leq x \leq 0.18$, and $0.195 \leq x \leq 0.205$, similar to the location of the transducer arrays for EA3. Interestingly enough, for both instruments pressure values around the highest P_{peak} reduced by more than 50% within a distance smaller or equal to about 2.5cm. On the opposite side, the most striking difference between the two instruments is the drastically higher (up to 2 or even 3 times) P_{peak} measurements for pressure transducers. These discrepancies could, in parts, be attributed to the disadvantages explicit to the pressure mapping system (e.g. lower digital resolution) and to calibration inaccuracies. However, the results presented in the previous section and mainly the comparison between EA2, EA1 and EA4 discussed above (see also Figure 6) indicate a strong effect related to the experimental set-up.

A favorable comparison between the P_{peak} map of the pressure system and the pressure transducer measurements can be seen in Figure 14. As expected for broken waves pressure peaks are randomly scattered and pressure magnitudes are significantly smaller than those for breaking waves. Nevertheless, for both instruments the highest P_{peaks} are reported for $y<0.15$ with maximum values of about 20kPa, which reduce to $P_{peak} \leq 16$ for $0.15 \leq y \leq 0.25$ and to less than 10kPa for $0.15<y$; similar results (not presented here) were found for NB and SP. In contradiction to the results presented in Figure 13 for breaking waves, a very good qualitative and quantitative agreement is seen for broken waves, Figure 14. P_{peak} measured for EA3 and broken waves were also found to be in-line to those for EA4 and therefore supporting the accuracy of the results presented in Figure 14.

Overall, the comparison of the peak pressure distribution recorded by the pressure mapping system and the matrix of pressure transducers shows a reasonably good, qualitative at the very least,

agreement and encourages the use of the *Tekscan I-Scan™* system for the acquisition of high resolution pressure maps.

3.1.3 Force measurements

The accuracy of the system is evaluated further in this subsection, where the force measured by the tactile sensor is compared with simultaneous load cell measurements. The force on the sensor is calculated as the integral of the pressures acting on each sensel with, however, the area considered for each measuring point (sensel) being larger (5.1x5.1mm) than the area over which the acting pressure is measured (approx. 3.1x3.1mm).

An example of the force time history as recorded by the load cell and the pressure mapping system, for the first reflected wave and the second and third breaking waves is shown in Figure 15. Despite small differences on the maximum force values reported, a good agreement is seen between the two time histories, especially with regards to the temporal location and shape of the force pulse. The peaks of the forces recorded for all 120 events for breaking and broken waves are compared in Figure 16.

The majority of the force values calculated for the tactile sensor ($F_{PSensor}$) range within ±20% of the load cell measurements (F_{PLC}), while 55% and 70% of these measurements are scattered between ±10%, for breaking and broken waves respectively. For only 9% and 5% (breaking and broken waves) of all measurements the force calculated for the tactile sensor differs by more than ±20% of the corresponding load cell results; similar results (not presented here) were acquired for NB and SP.

For the pressure mapping system, the above mentioned discrepancies can be attributed to sensel (pressure) calibration inaccuracies and to errors introduced by the calculation of the applied force as the integral of pressures acting on parts of and not over the whole sensor. Nevertheless with the majority of the errors ranging within ±20% the performance of the *Tekscan I-scan™* system is deemed satisfactory. In addition, the force results presented provide further support to the argument that the drastic disagreement between pressure peaks presented in section 3.1.2 for the tactile sensor and pressure transducers are mainly due to the differences in the experimental set-ups EA1 and EA3.

4 Conclusions

This work looks at the details of the application of the *Tekscan I-Scan™* pressure mapping system in hydraulic model tests involving wave impacts on rigid structures. The system is described and an appropriate experimental set-up and calibration methodology are proposed. The pressure mapping system is used to measure wave impact induced pressures and loads on a model seawall and the results are used to validate the system against pressure transducer and load cell measurements.

The comparison of pressure mapping system with pressure transducer measurements reveals a good agreement between both the pressure pulse time histories and peak pressure (P_{peak}) magnitudes. With regards to the former, high frequency pressure oscillations, potentially, related to the presence of bubbles are not captured by the system. With respect to P_{peak} and for all (four) breaker types considered, the least good agreement is observed for pressures closer the lower end of the nominal range of the tactile sensor used. Differences between the system and pressure transducer measurements for the mean and std of P_{peak} range between ±15%, while the average values of the 3, 5 and 10 highest P_{peak} differ by up to ±10%.

An encouraging agreement for the spatial distribution (horizontal and vertical) of P_{peak} is also reported. The highest P_{peak} is recorded at similar locations and the reduction trends shown for adjacent pressures agree equally well. It is noteworthy that for breaking waves, the significantly higher pressure transducer measurements are due to differences in the experimental set-up.

On the contrary, the pressure mapping system in combination with the tactile sensor (model 9500) used reports shorter rise times (t_r) than pressure transducers; this trend is more pronounced for the strongest impacts. Nonetheless, a good qualitative agreement on the $P_{peak} - t_r$ relation is demonstrated

and the overall differences are not considered significant enough to disregard the use of the system. In support of the latter, the integral of pressures acting on the tactile sensor -the force applied over the whole sensor- differ from simultaneous load cell measurements by less than ±20%. In addition, thermal and/or medium change related signal drifts, similar to those reported in the literature, are not seen to occur for the short application times of wave impact induced pressures.

In summary, the experimental results presented here encourage the use of the *Tekscan I-Scan™* pressure mapping system in combination with the experimental set-up and the calibration methodology suggested. Potential users, however, should be aware that applying the system in hydraulic model tests involving breaking waves can be laborious and requires careful planning and cautious use. It is also noted that to the authors' opinion the system, with its current limitations, does not constitute an alternative to pressure transducers but it has the capacity to provide unique information on the spatial distribution of impact induced pressures. Further research efforts can therefore be dedicated on the combined use of the pressure mapping system and pressure transducers. As an example the pressure mapping system can be used initially to highlight the location of high/extreme pressures and then pressure transducers can be deployed to collect pressure measurements at a higher sampling frequency and digital resolution.

5 Acknowledgement

These experiments have been supported by the European Commission 7th Framework Programme project HyRes under the HYDRALAB IV network, contract no. 261520. The second author also acknowledges the support of the European Community's 7th Framework Programme through the transnational access grants of the HYDRALAB IV activity. Prof. Jens Peter Kofoed, Dr. Arthur Pecher and Dr. Matthias Kudella are especially thanked for their generous contribution in prior projects leading to the development or the required experience. This research was also aided by the Ministry of Education of Spain (FPU grant AP-2010-4641). Finally, the personnel of the CIEMLAB at the LIM-UPC (Barcelona).

6 References

Baer, T.E., Pedersen, D. R., Rudert, M. J., Vos, N. A., Grosland, N. M., Brown, T. D. (2004). Calibrating and monitoring sheet array pressure sensors for intra-articular load measurement. In and E. Societies of Canada, USA, Japan, ed. *Proceedings of the Fifth Combined Meeting of the Orthopaedic Research*. p. 115.

Brimacombe, J.M., Wilson, D.R., Hodgson, A.J, Ho, K.C., Anglin C. (2009). Effect of calibration method on Tekscan sensor accuracy. *Journal of biomechanical engineering*, 131(3), 034503. doi:10.1115/1.3005165

Bullock, G. N., Obhrai, C., Peregrine, D. H., & Bredmose, H. (2007). Violent breaking wave impacts. Part 1: Results from large-scale regular wave tests on vertical and sloping walls. *Coastal Engineering*, *54*(8), 602–617. doi:10.1016/j.coastaleng.2006.12.002

Cuomo, G., Allsop, N. W. H., Bruce, T., & Pearson, J. (2010). Breaking wave loads at vertical seawalls and breakwaters. *Coastal Engineering*, *57*(4), 424–439. doi:10.1016/j.coastaleng.2009.11.005

Hattori, M., Arami, A., & Yui, T. (1994). Wave impact pressure on vertical walls under breaking waves of various types. *Coastal Engineering*, *22*(1-2), 79–114. doi:10.1016/0378-3839(94)90049-3

Hofland, B., Lech Kaminski, M., & Wolters, G. (2010). LARGE SCALE WAVE IMPACTS ON A VERTICAL WALL. *Proceedings of the 25th Coastal Engineering Conference*.

Hull, P., & Müller, G. (2002). An investigation of breaker heights, shapes and pressures. *Ocean Engineering*, *29*, 59–79. doi:10.1016/S0029-8018(00)00075-5

Kim, S.-Y., Kim, K.-H., & Kim, Y. (2015). Comparative study on pressure sensors for sloshing experiment. *Ocean Engineering*, *94*, 199–212. doi:10.1016/j.oceaneng.2014.11.014

Kisacik, D., Troch, P., & Philippe Van Bogaert. (2012). Experimental study of pressure distributions due to the breaking wave impacts. *Coastal Engineering*.

Marzeddu, A., Gironella, X., & Conejo, A. S. (2013). Impulsive wave loads on rigid structures , an experimental approach. *Journal of Coastal Research*, (65). doi:10.2112/SI65-xxx.1

Marzeddu, A., Gironella, X., Sánchez-Arcilla, A., & Sutherland, J. (2014). Laboratory effects on measuring impact loads on rigid coastal structures. In *Proceedings of the 3rd IAHR Europe Congress, 2014, Porto-Portugal*.

Oumeraci, H., Allsop, N. W. H., De Groot, M., Crouch, R., Voortman, H., & Vrijling, H. (2001). *Probabilistic design tools for vertical breakwaters*. (A. kortenhaus & H. Voortman, Eds.). Amsterdam : (ndl): Swets & Zeitlinger,.

Peregrine, D. H. (2003). Water - Wave Impact on walls. *Annual Review of Fluid Mechanics*, *35*(1939), 23–43. doi:10.1146/annurev.fluid.35.101101.161153

Ramachandran, K., Schimmels, S., Stagonas, D., & Müller, G. (2013). Measuring Wave Impact on Coastal Structures with High Spatial and Temporal Resolution--Tactile Pressure Sensors a Novel Approach. In *35th IAHR World Congress, Chengdu, China*.

Saruwatari, A., Watanabe, Y., & Ingram, D. M. (2009). Scarifying and fingering surfaces of plunging jets. *Coastal Engineering*, *56*, 1109–1122. doi:10.1016/j.coastaleng.2009.08.007

Stansberg, C., Berget, K., Graczyk, M., Muthanna, C., & Pakozdi, C. (2012). Breaking wave kinematics and resulting slamming pressures on a vertical column. In *Proceedings of the ASME 2012 31st International Conference on Ocean, Offshore and Arctic Engineering*. Rio de Janeiro, Brazil.

Tekscan, I. (2008). I-Scan and High speed I-Scan User manual, 1–11.

Figure

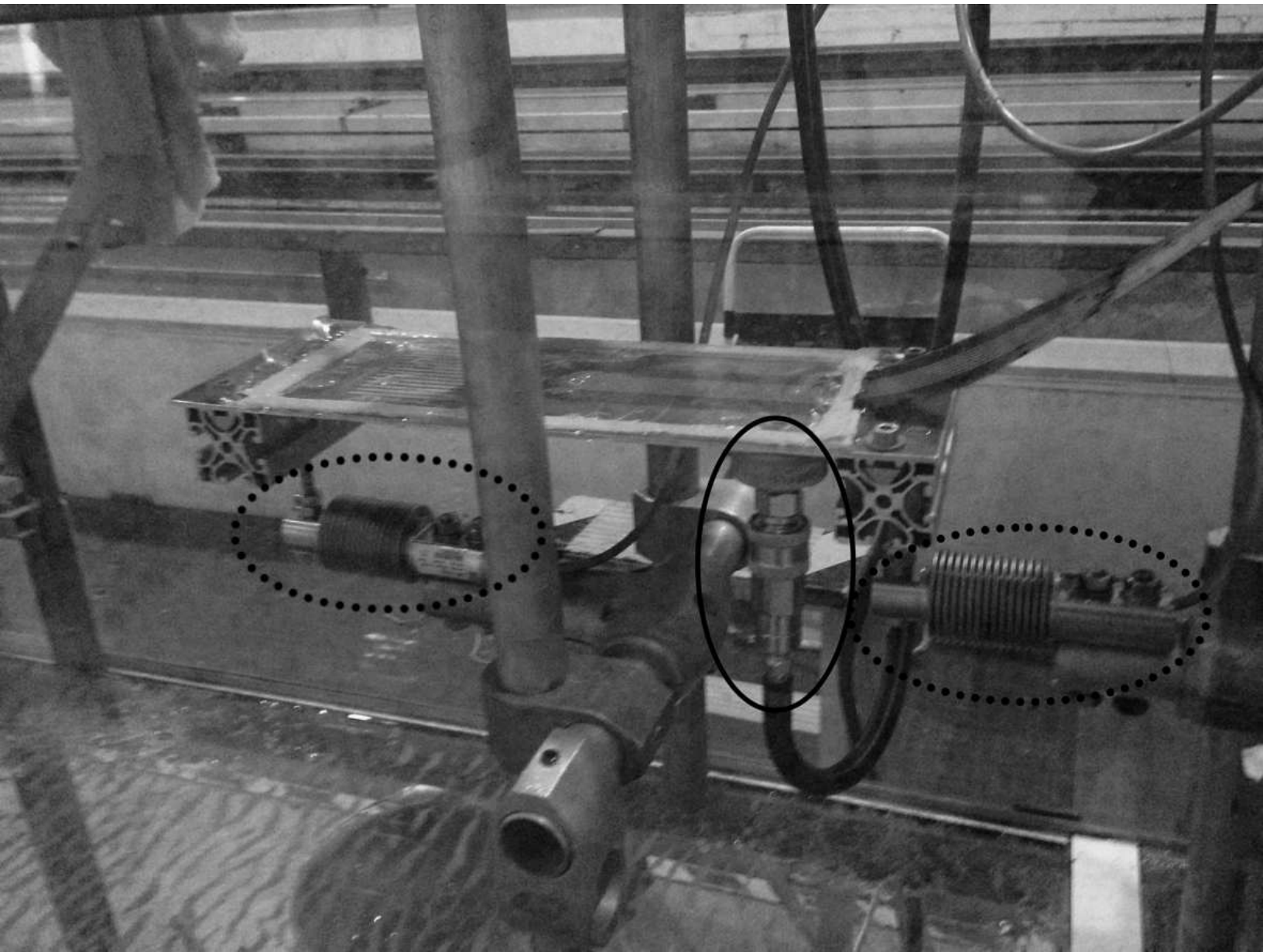

Figure

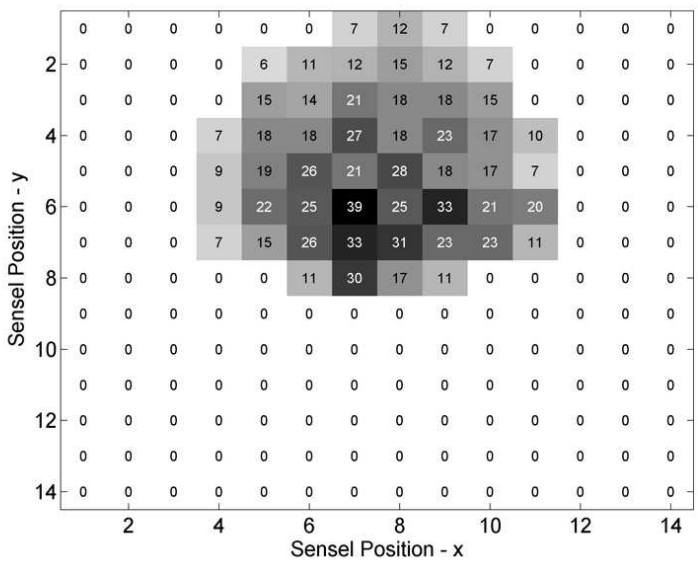
Sensel Position - y
Sensel Position - x
2
4
6
8
10
12
14

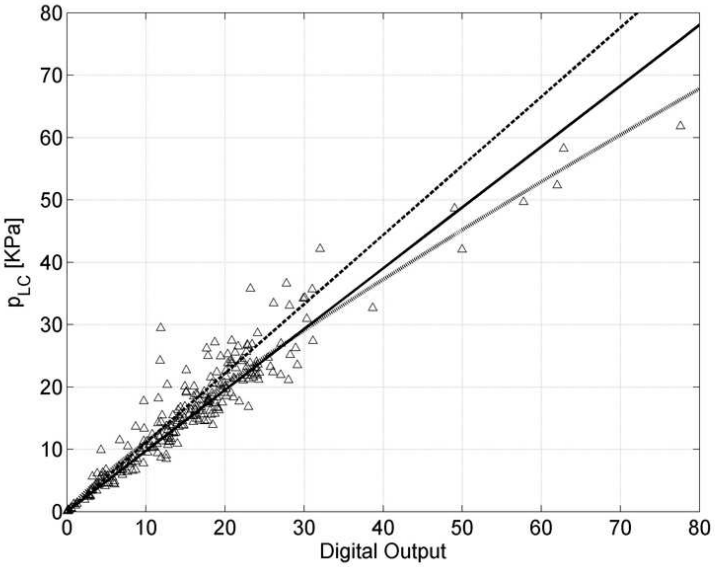
p_{LC} [KPa]
Digital Output
0
10
20
30
40
50
60
70
80

Figure

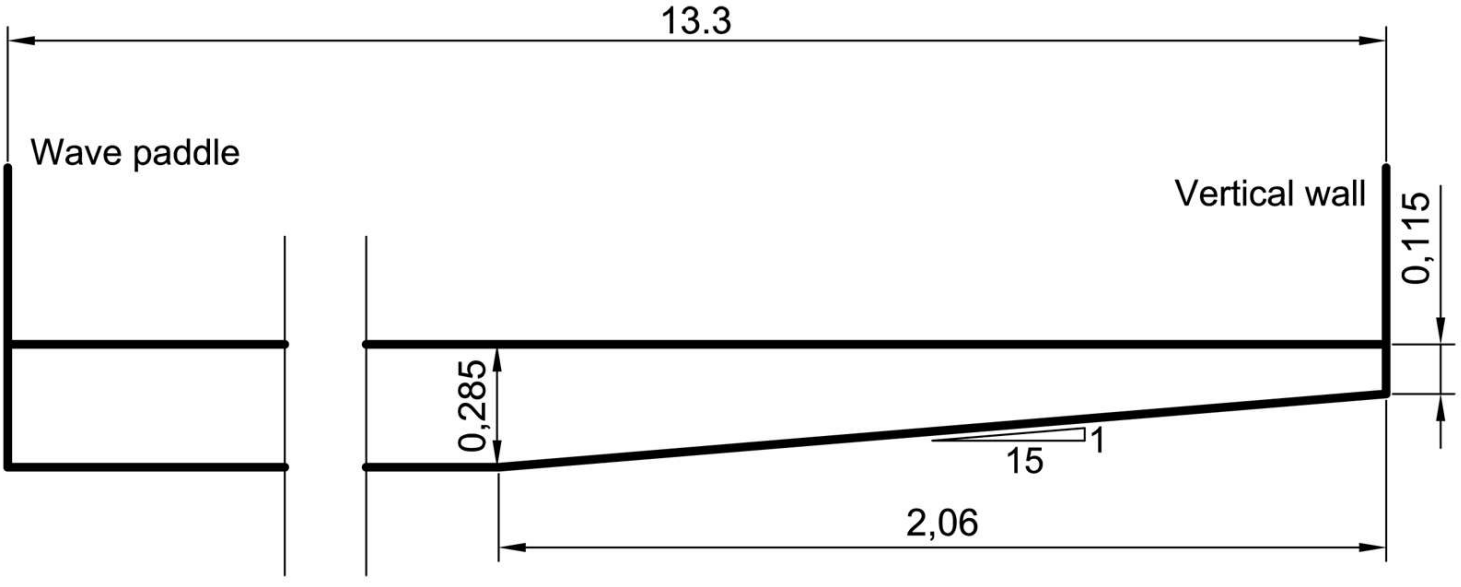

Figure

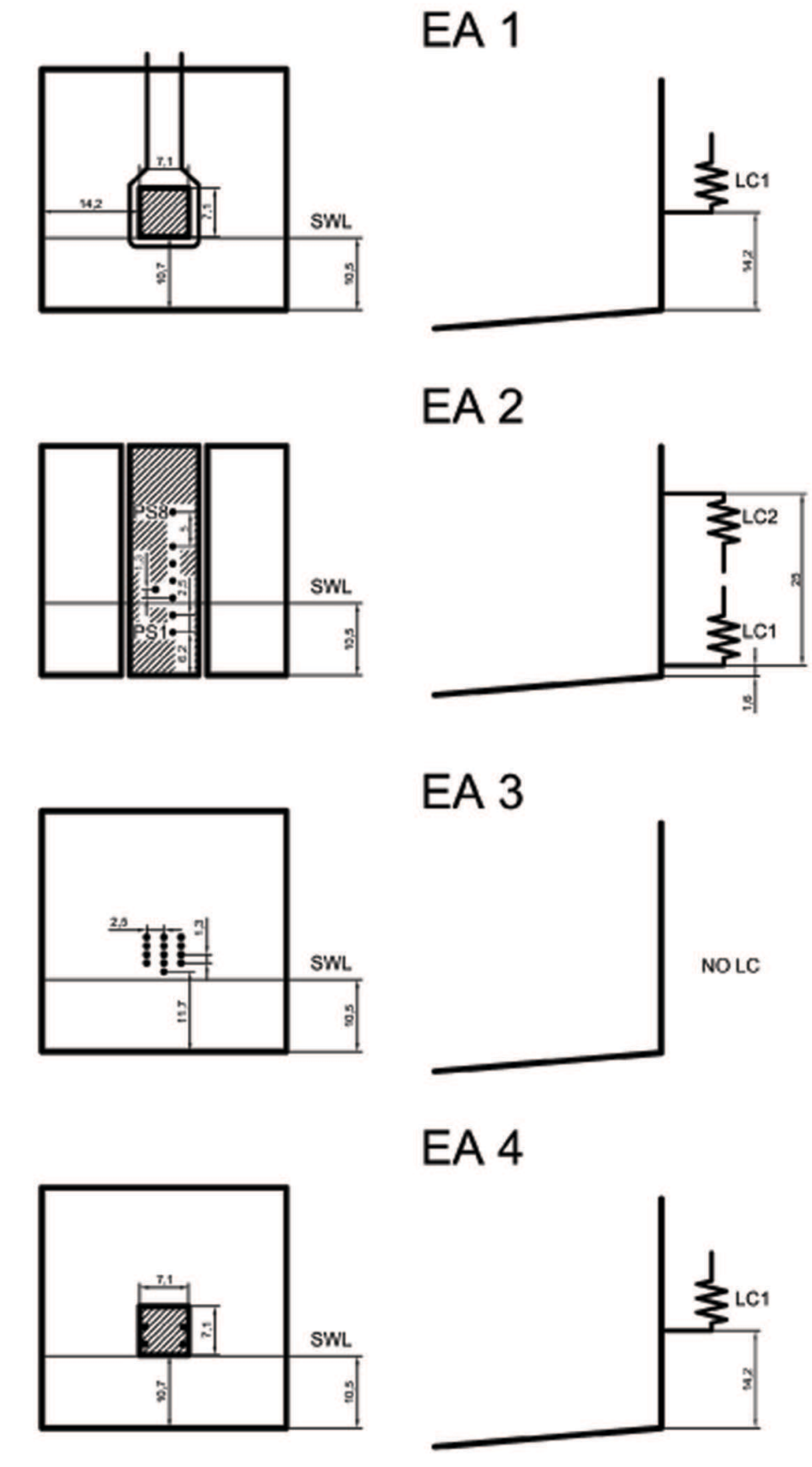
EA 1
7.1
14.2
7.1
SWL
10.7
10.5
LC1
14.2
EA 2
S2
S1
SWL
10.5
LC2
LC1
20
1.6
EA 3
2.0
1.3
SWL
11.7
10.5
NO LC
EA 4
7.1
7.1
SWL
10.7
10.5
LC1
14.2
Load cell measurement area
Load cell
PMS
Pressure transducers

Figure

BREAKING WAVE

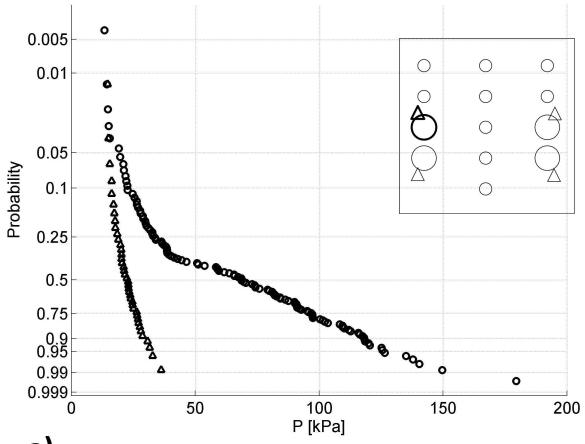

a)

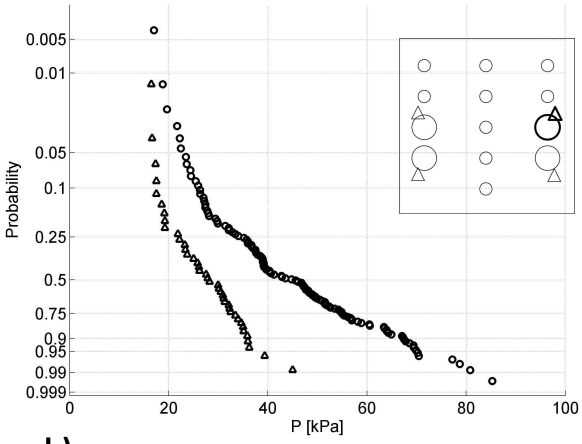

b)

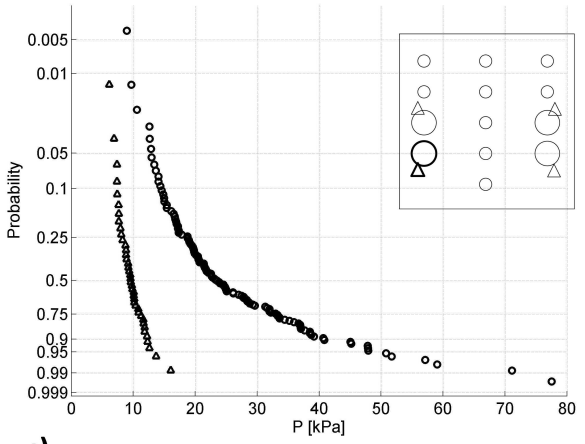

c)

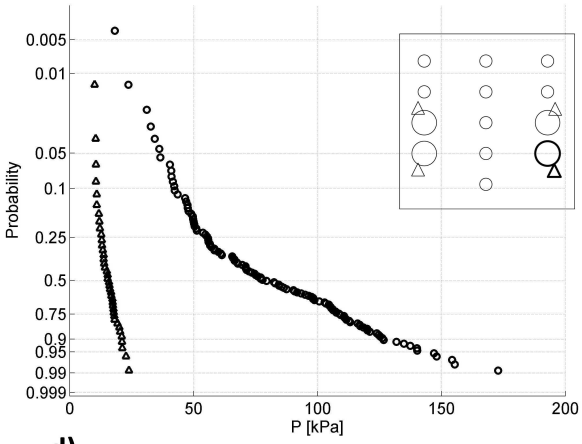

d)

BROKEN WAVE

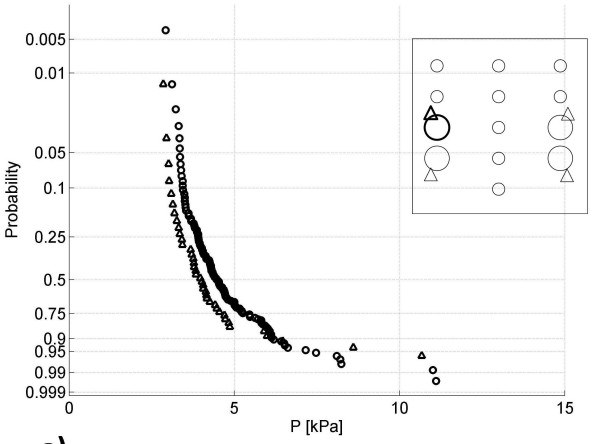

a)

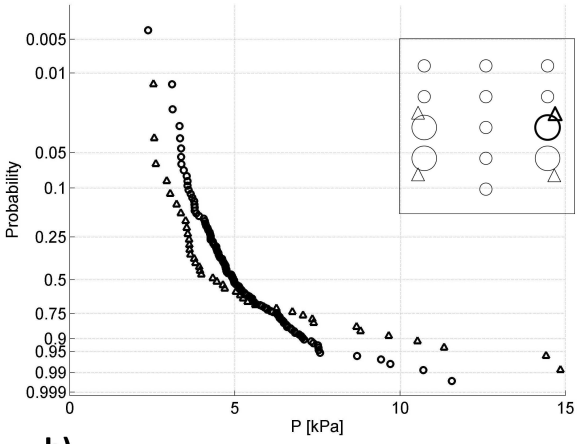

b)

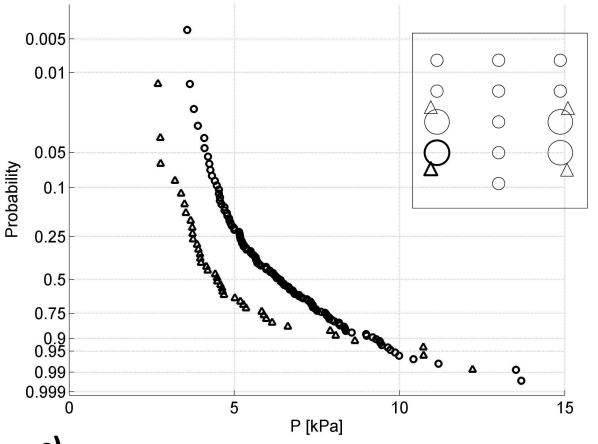

c)

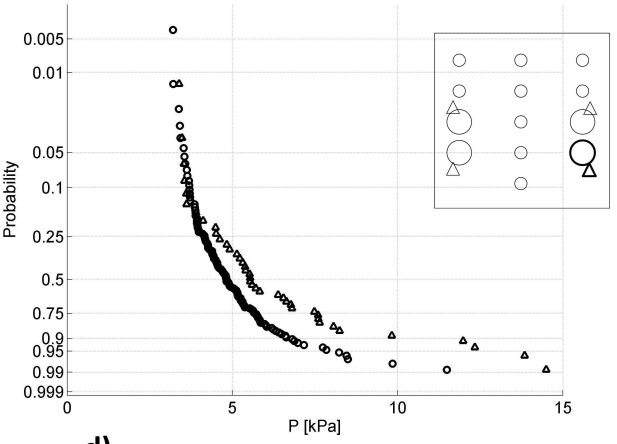

d)

Figure

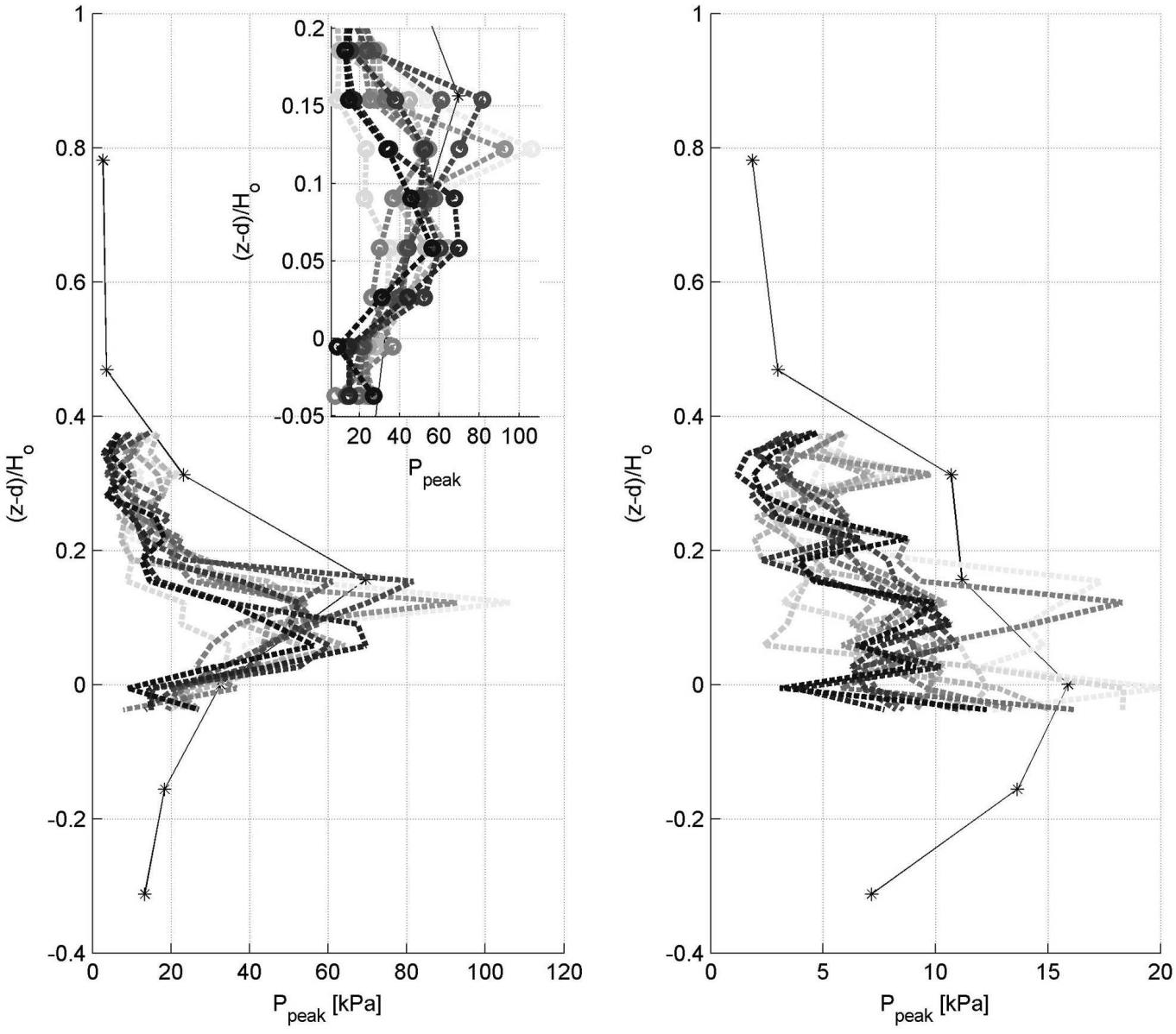
(z-d)/H_o
P_peak [kPa]
P_peak
1
0.8
0.6
0.4
0.2
0
-0.2
-0.4
0
20
40
60
80
100
120
0.2
0.15
0.1
0.05
-0.05
5
10
15

Figure

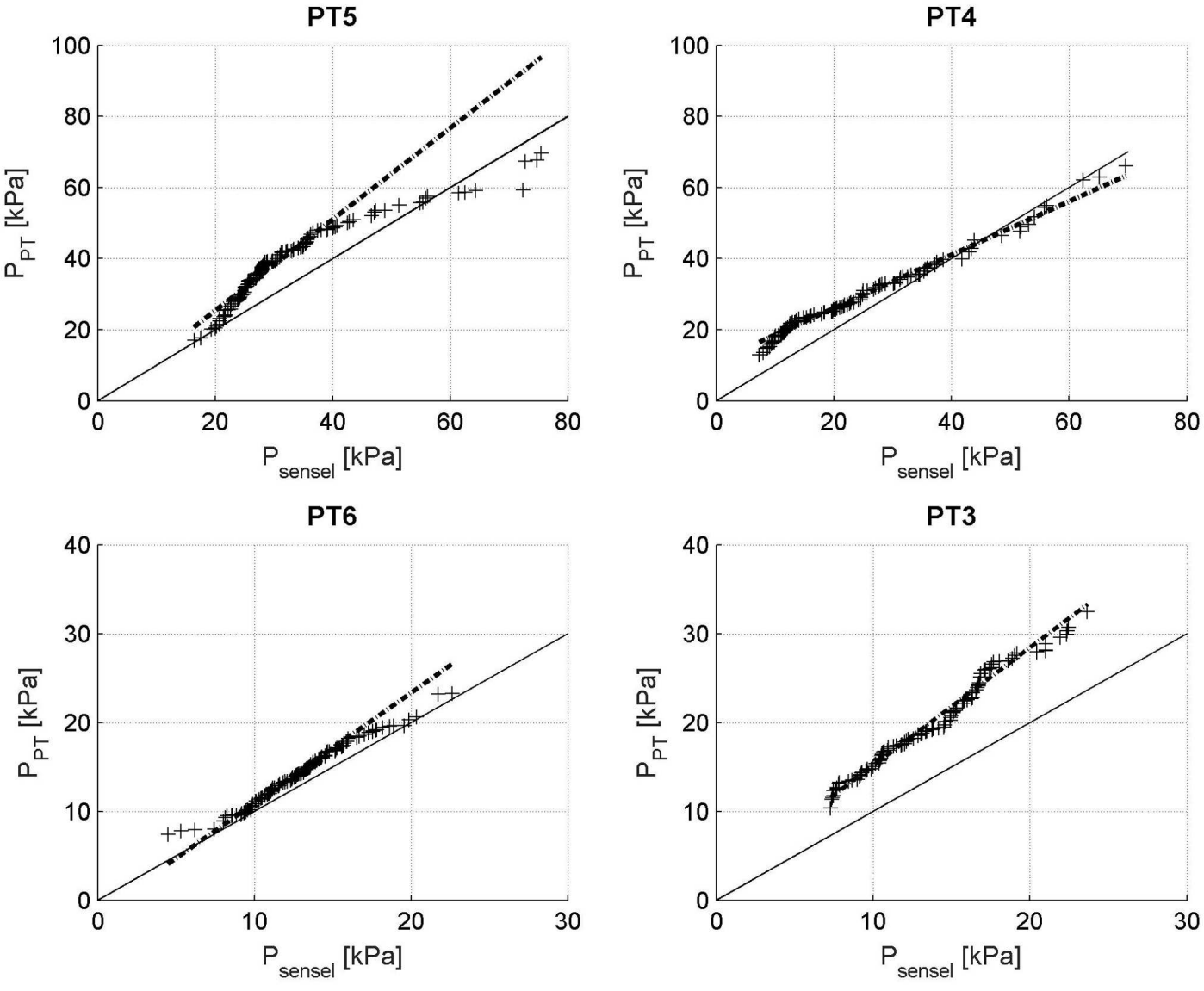

Figure

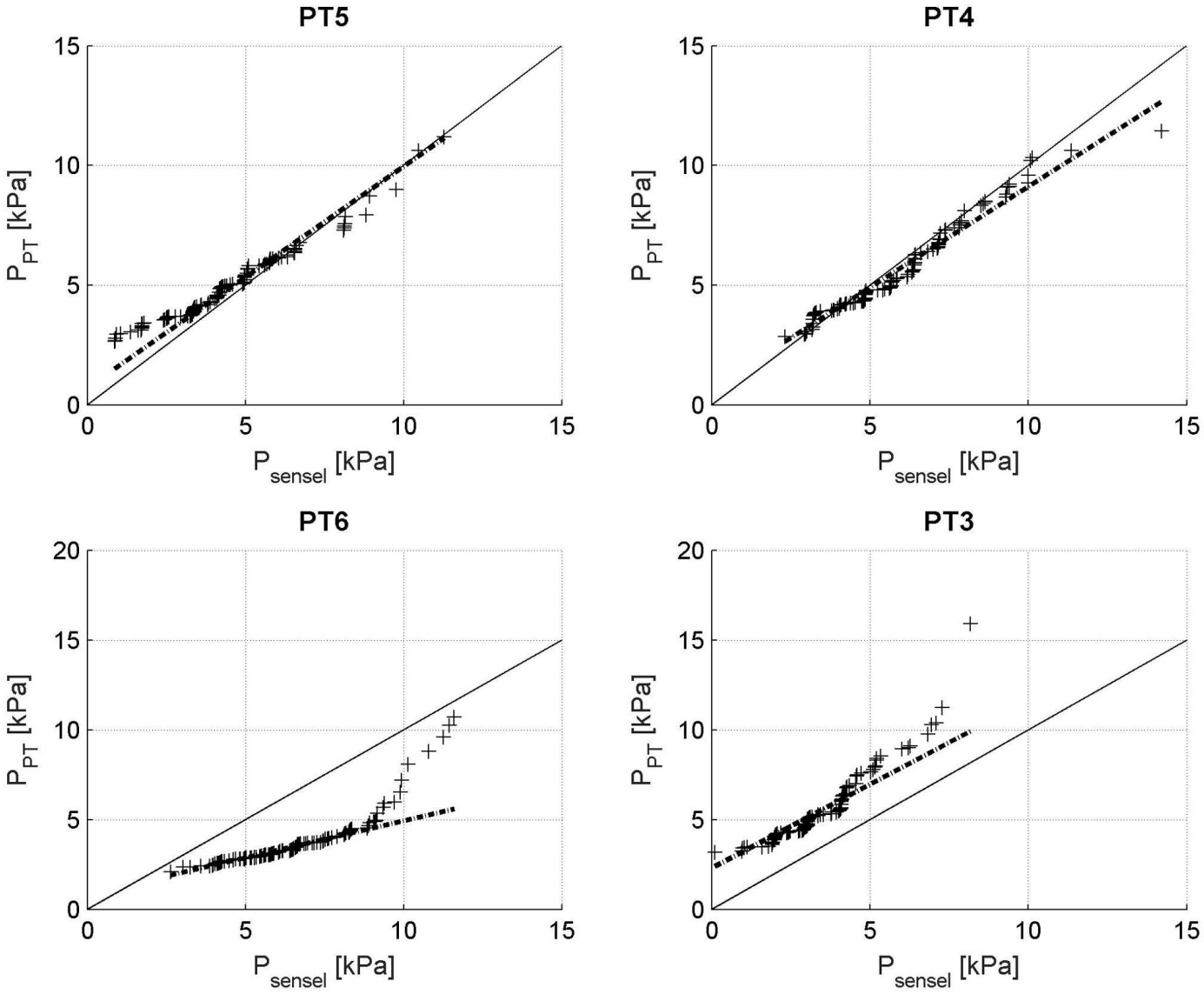

Figure

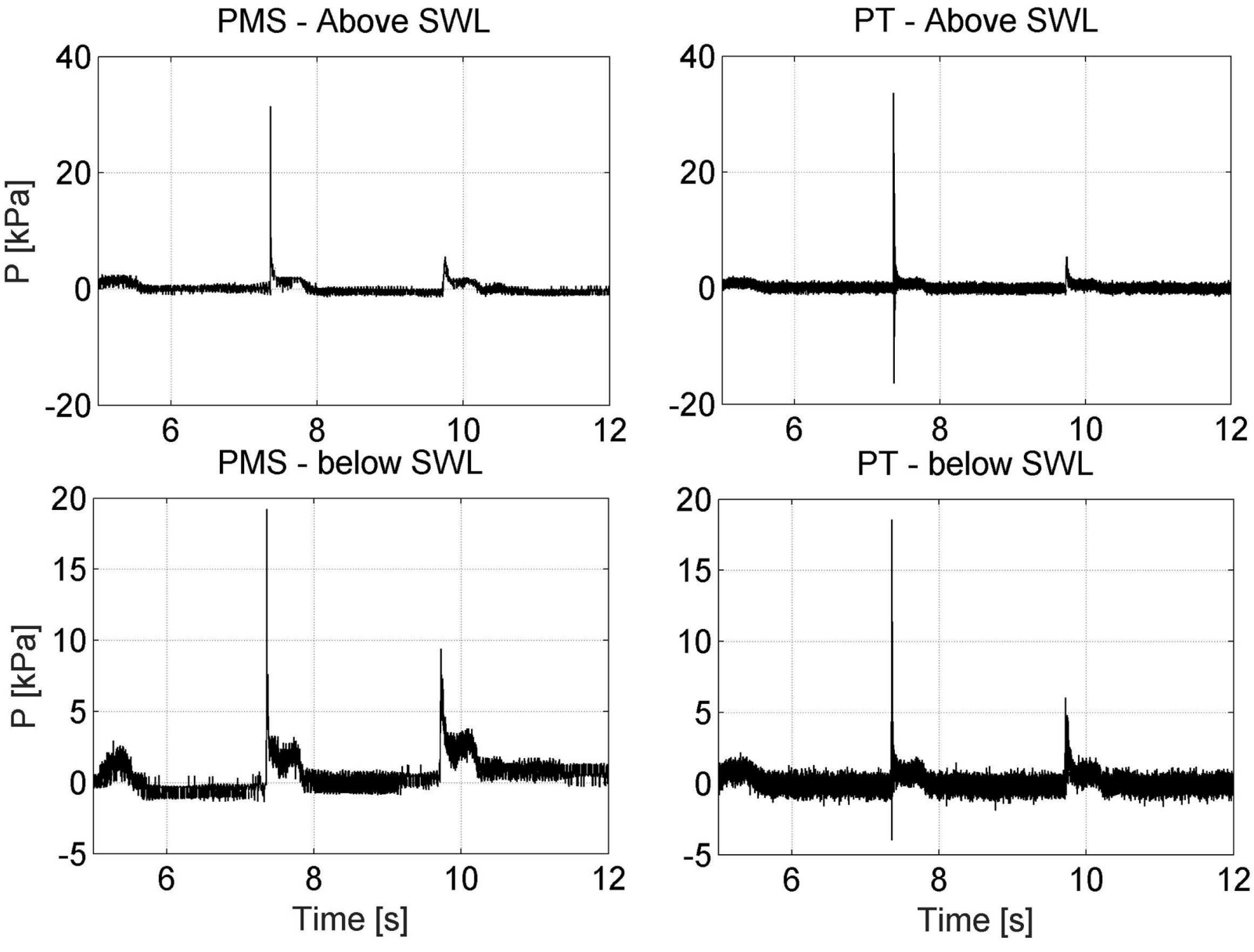
PMS - Above SWL
PT - Above SWL
PMS - below SWL
PT - below SWL
P [kPa]
Time [s]
40
20
0
-20
15
10
5
-5
6
8
10
12

Figure

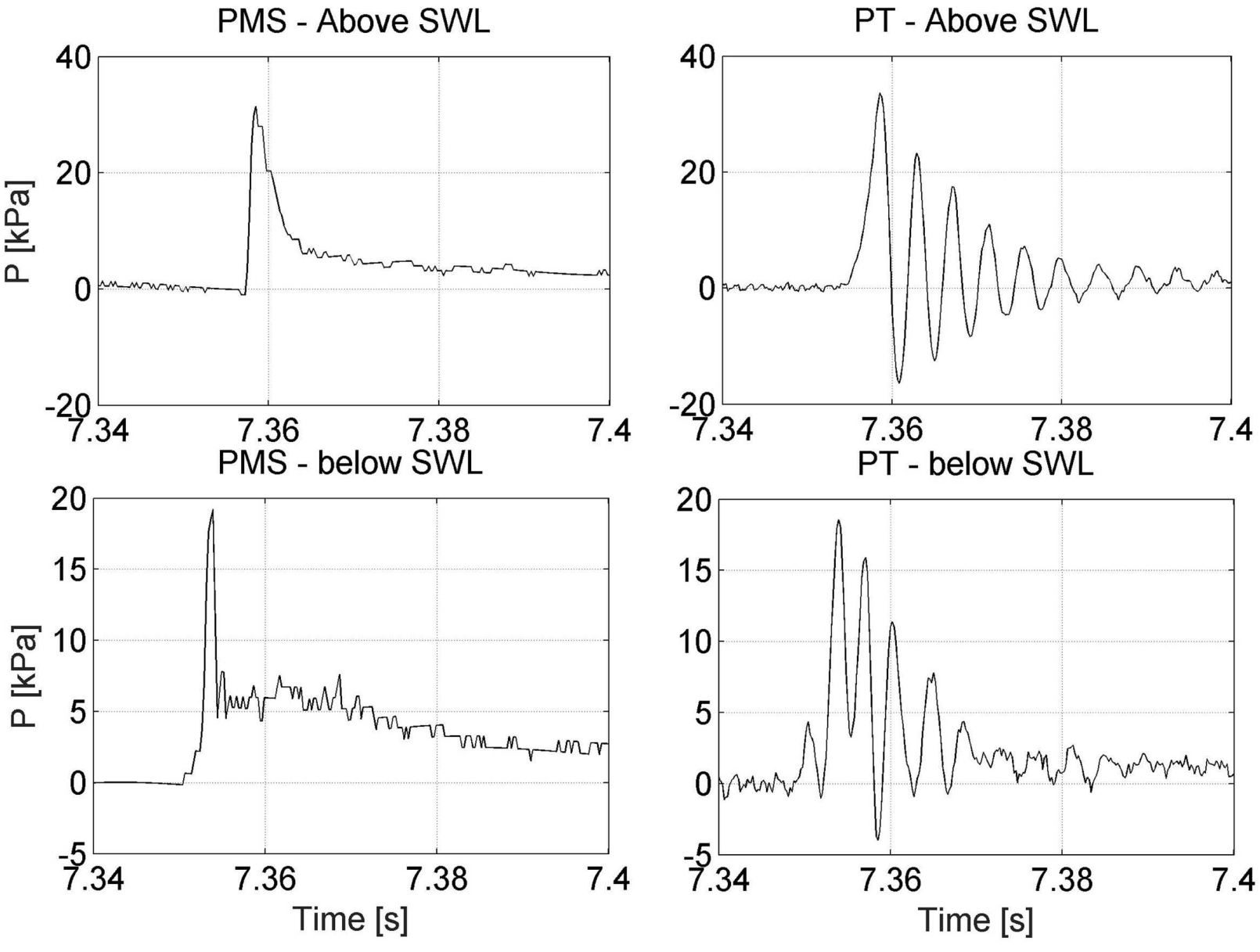
PMS - Above SWL
PT - Above SWL
PMS - below SWL
PT - below SWL
P [kPa]
Time [s]
40
20
0
-20
15
10
5
-5
7.34
7.36
7.38
7.4

Figure

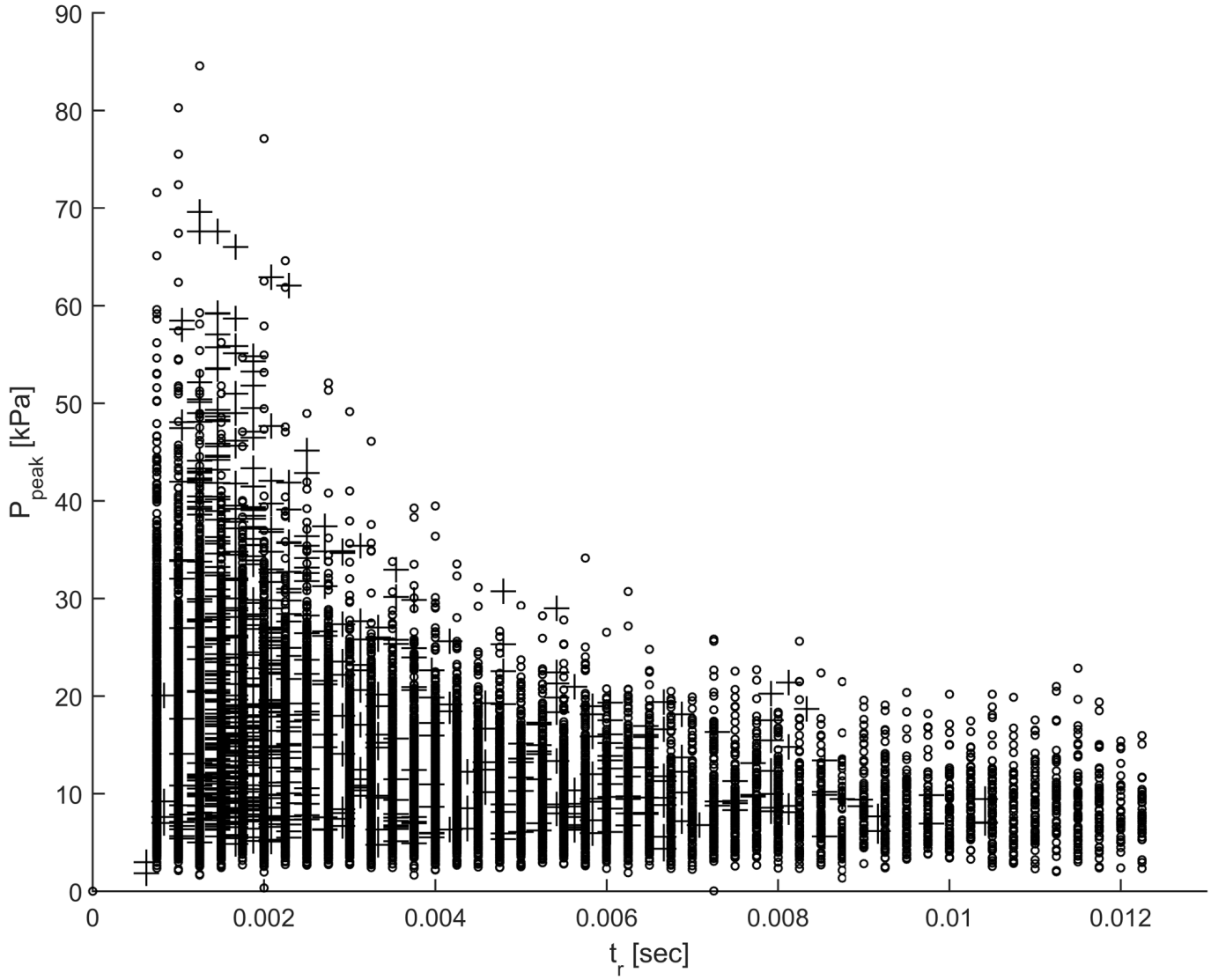
90
80
70
60
50
40
30
20
10
0
P peak [kPa]
0
0.002
0.004
0.006
0.008
0.01
0.012
t r [sec]

Figure

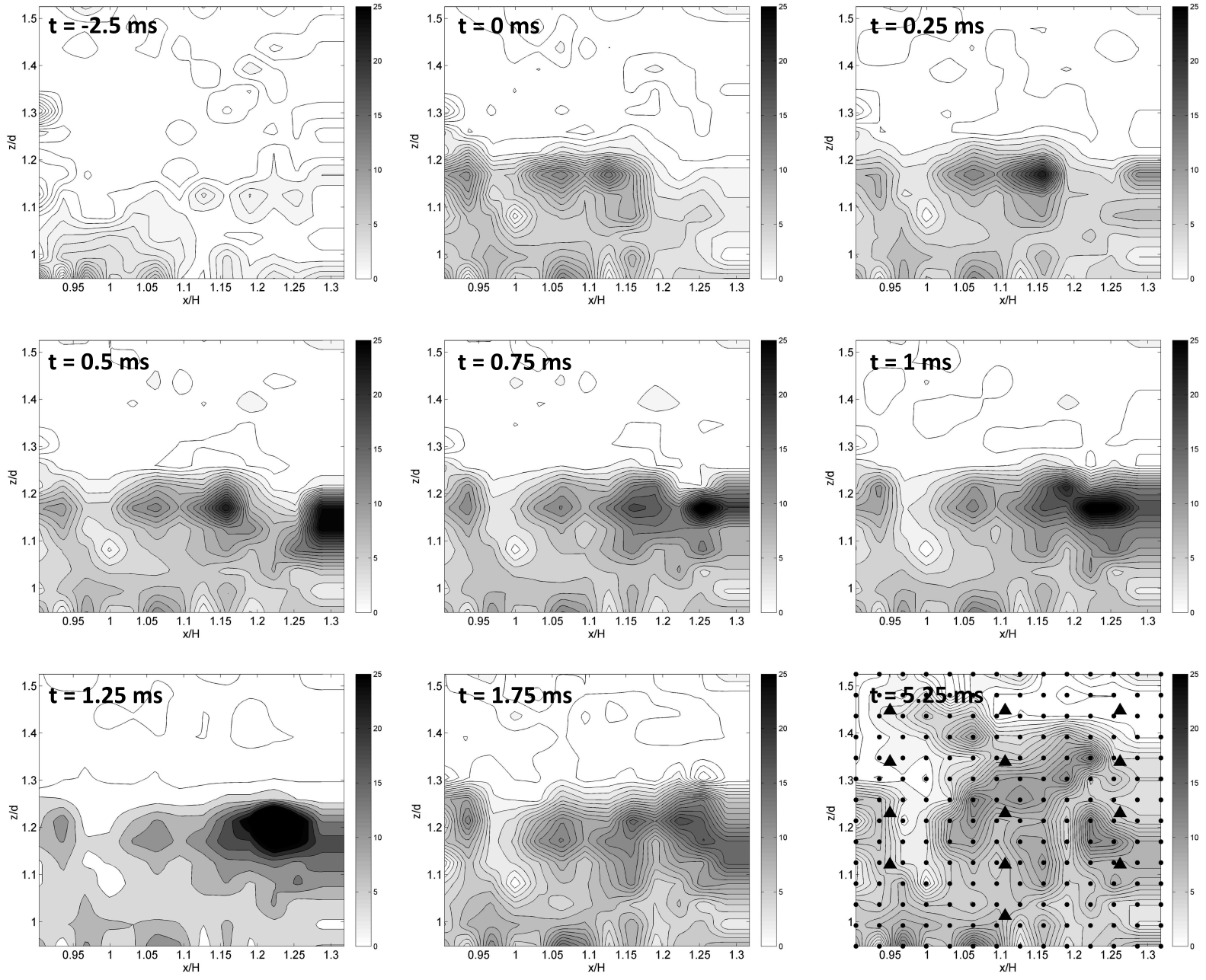
t = -2.5 ms
t = 0 ms
t = 0.25 ms
t = 0.5 ms
t = 0.75 ms
t = 1 ms
t = 1.25 ms
t = 1.75 ms
t = 5.25 ms
z/d
x/H
0.95 1 1.05 1.1 1.15 1.2 1.25 1.3
1 1.1 1.2 1.3 1.4 1.5
0 5 10 15 20 25

Figure

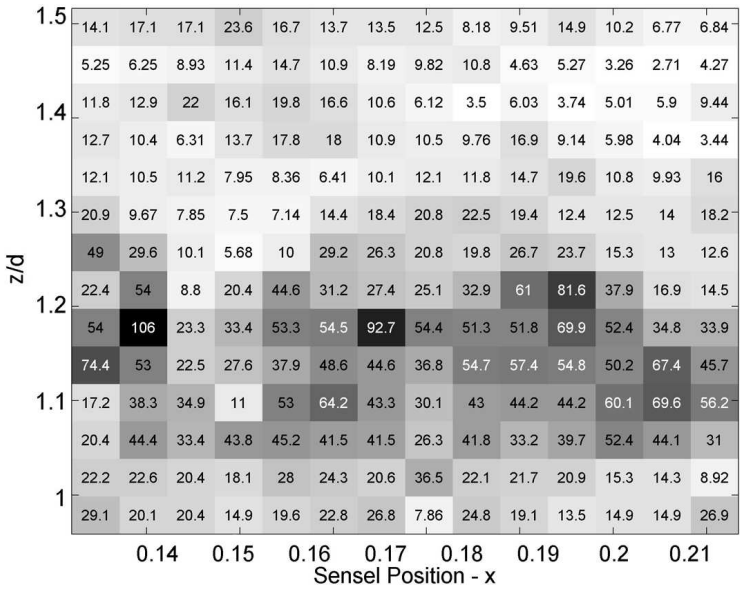
z/d
1.5
1.4
1.3
1.2
1.1
1
14.1 17.1 17.1 23.6 16.7 13.7 13.5 12.5 8.18 9.51 14.9 10.2 6.77 6.84
5.25 6.25 8.93 11.4 14.7 10.9 8.19 9.82 10.8 4.63 5.27 3.26 2.71 4.27
11.8 12.9 22 16.1 19.8 16.6 10.6 6.12 3.5 6.03 3.74 5.01 5.9 9.44
12.7 10.4 6.31 13.7 17.8 18 10.9 10.5 9.76 16.9 9.14 5.98 4.04 3.44
12.1 10.5 11.2 7.95 8.36 6.41 10.1 12.1 11.8 14.7 19.6 10.8 9.93 16
20.9 9.67 7.85 7.5 7.14 14.4 18.4 20.8 22.5 19.4 12.4 12.5 14 18.2
49 29.6 10.1 5.68 10 29.2 26.3 20.8 19.8 26.7 23.7 15.3 13 12.6
22.4 54 8.8 20.4 44.6 31.2 27.4 25.1 32.9 61 81.6 37.9 16.9 14.5
54 106 23.3 33.4 53.3 54.5 92.7 54.4 51.3 51.8 69.9 52.4 34.8 33.9
74.4 53 22.5 27.6 37.9 48.6 44.6 36.8 54.7 57.4 54.8 50.2 67.4 45.7
17.2 38.3 34.9 11 53 64.2 43.3 30.1 43 44.2 44.2 60.1 69.6 56.2
20.4 44.4 33.4 43.8 45.2 41.5 41.5 26.3 41.8 33.2 39.7 52.4 44.1 31
22.2 22.6 20.4 18.1 28 24.3 20.6 36.5 22.1 21.7 20.9 15.3 14.3 8.92
29.1 20.1 20.4 14.9 19.6 22.8 26.8 7.86 24.8 19.1 13.5 14.9 14.9 26.9
0.14 0.15 0.16 0.17 0.18 0.19 0.2 0.21
Sensel Position - x

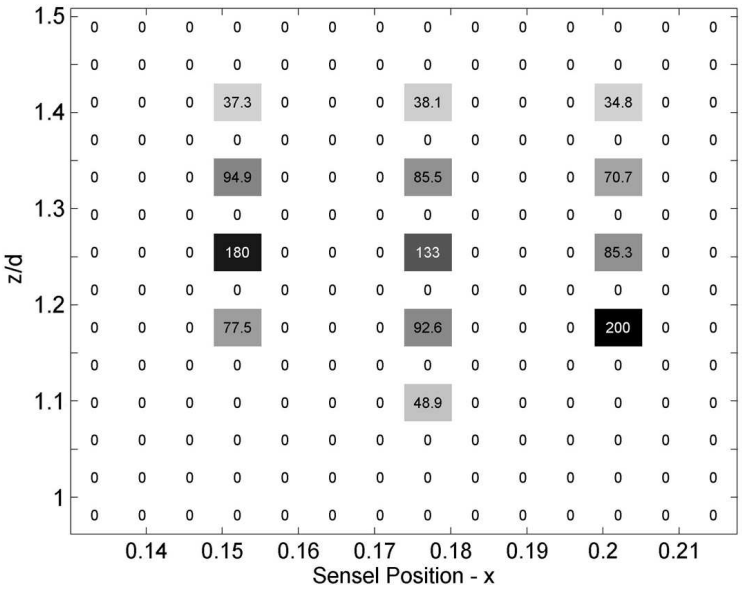
z/d
1.5
1.4
1.3
1.2
1.1
1
0 0 0 0 0 0 0 0 0 0 0 0 0 0
0 0 0 0 0 0 0 0 0 0 0 0 0 0
0 0 0 37.3 0 0 0 38.1 0 0 0 34.8 0 0
0 0 0 0 0 0 0 0 0 0 0 0 0 0
0 0 0 94.9 0 0 0 85.5 0 0 0 70.7 0 0
0 0 0 0 0 0 0 0 0 0 0 0 0 0
0 0 0 180 0 0 0 133 0 0 0 85.3 0 0
0 0 0 0 0 0 0 0 0 0 0 0 0 0
0 0 0 77.5 0 0 0 92.6 0 0 0 200 0 0
0 0 0 0 0 0 0 0 0 0 0 0 0 0
0 0 0 0 0 0 0 48.9 0 0 0 0 0 0
0 0 0 0 0 0 0 0 0 0 0 0 0 0
0 0 0 0 0 0 0 0 0 0 0 0 0 0
0 0 0 0 0 0 0 0 0 0 0 0 0 0
0.14 0.15 0.16 0.17 0.18 0.19 0.2 0.21
Sensel Position - x

Figure

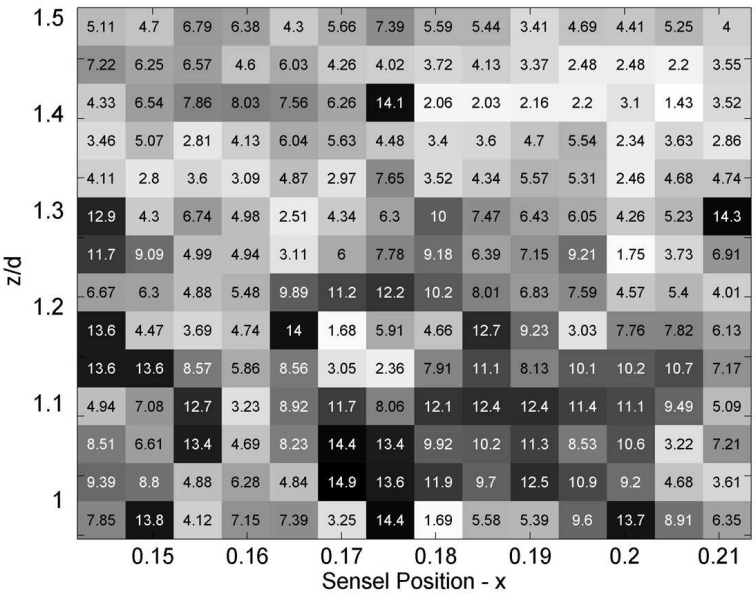
z/d
1.5
1.4
1.3
1.2
1.1
1
5.11 4.7 6.79 6.38 4.3 5.66 7.39 5.59 5.44 3.41 4.69 4.41 5.25 4
7.22 6.25 6.57 4.6 6.03 4.26 4.02 3.72 4.13 3.37 2.48 2.48 2.2 3.55
4.33 6.54 7.86 8.03 7.56 6.26 14.1 2.06 2.03 2.16 2.2 3.1 1.43 3.52
3.46 5.07 2.81 4.13 6.04 5.63 4.48 3.4 3.6 4.7 5.54 2.34 3.63 2.86
4.11 2.8 3.6 3.09 4.87 2.97 7.65 3.52 4.34 5.57 5.31 2.46 4.68 4.74
12.9 4.3 6.74 4.98 2.51 4.34 6.3 10 7.47 6.43 6.05 4.26 5.23 14.3
11.7 9.09 4.99 4.94 3.11 6 7.78 9.18 6.39 7.15 9.21 1.75 3.73 6.91
6.67 6.3 4.88 5.48 9.89 11.2 12.2 10.2 8.01 6.83 7.59 4.57 5.4 4.01
13.6 4.47 3.69 4.74 14 1.68 5.91 4.66 12.7 9.23 3.03 7.76 7.82 6.13
13.6 13.6 8.57 5.86 8.56 3.05 2.36 7.91 11.1 8.13 10.1 10.2 10.7 7.17
4.94 7.08 12.7 3.23 8.92 11.7 8.06 12.1 12.4 12.4 11.4 11.1 9.49 5.09
8.51 6.61 13.4 4.69 8.23 14.4 13.4 9.92 10.2 11.3 8.53 10.6 3.22 7.21
9.39 8.8 4.88 6.28 4.84 14.9 13.6 11.9 9.7 12.5 10.9 9.2 4.68 3.61
7.85 13.8 4.12 7.15 7.39 3.25 14.4 1.69 5.58 5.39 9.6 13.7 8.91 6.35
0.15 0.16 0.17 0.18 0.19 0.2 0.21
Sensel Position - x

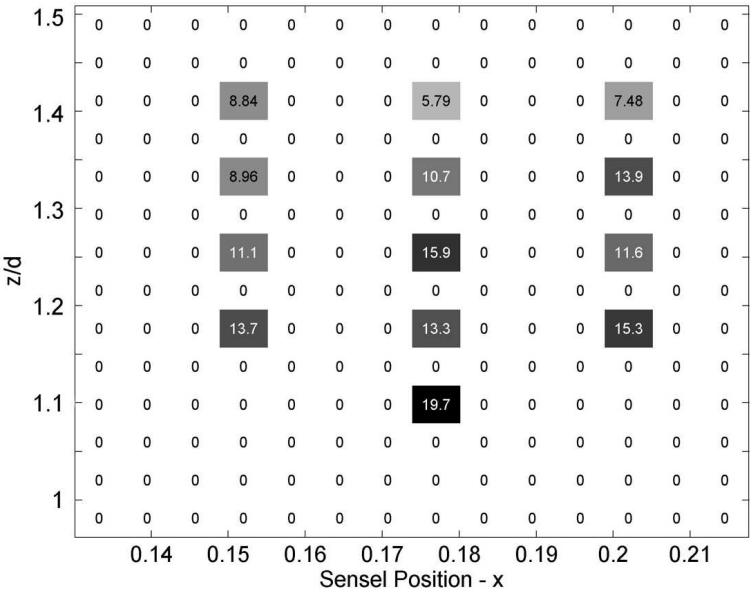
z/d
1.5
1.4
1.3
1.2
1.1
1
8.84 5.79 7.48
8.96 10.7 13.9
11.1 15.9 11.6
13.7 13.3 15.3
19.7
0.14 0.15 0.16 0.17 0.18 0.19 0.2 0.21
Sensel Position - x

Figure

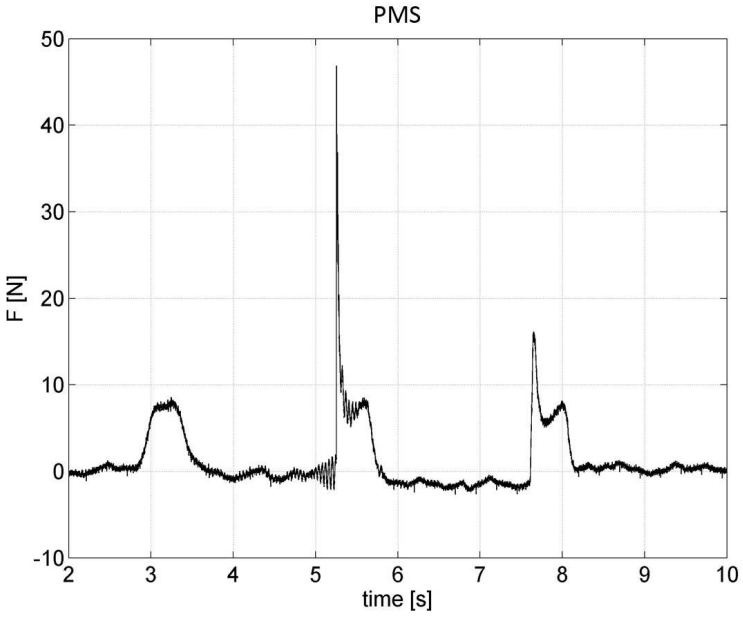
PMS
F [N]
time [s]
50
40
30
20
10
0
-10
2
3
4
5
6
7
8
9
10

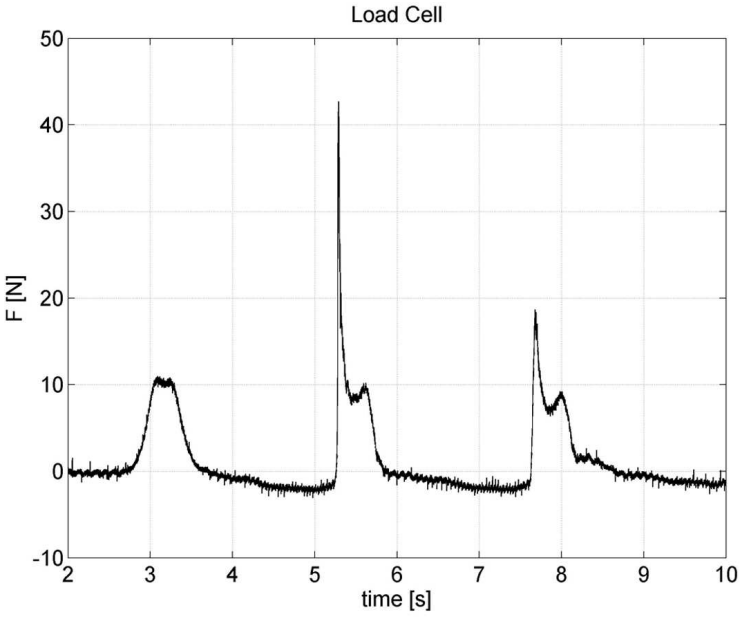
Load Cell
F [N]
time [s]
50
40
30
20
10
0
-10
2
3
4
5
6
7
8
9
10

Figure

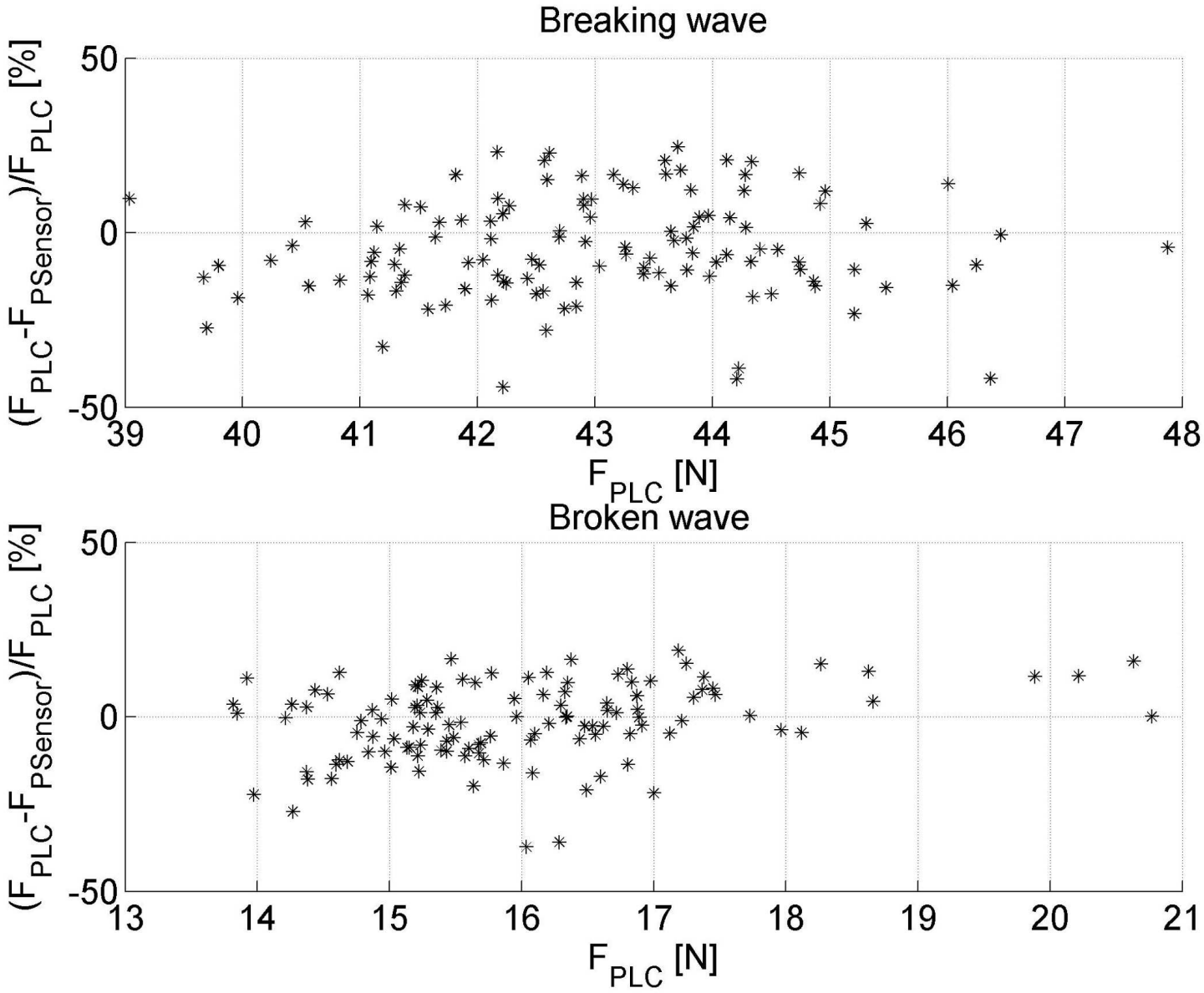
Breaking wave
(F_PLC-F_PSensor)/F_PLC [%]
50
0
-50
39
40
41
42
43
44
45
46
47
48
F_PLC [N]
Broken wave
(F_PLC-F_PSensor)/F_PLC [%]
50
0
-50
13
14
15
16
17
18
19
20
21
F_PLC [N]